Chemical Science

EDGE ARTICLE

View Article Online
View Journal | View Issue

CrossMark click for updates

Cite this: *Chem. Sci.*, 2014, **5**, 3795

Published on 16 June 2014. Downloaded by Tamkang University Libraries on 14/04/2015 07:55:44.

Hammett correlations as test of mechanism of CO-induced disulfide elimination from dinitrosyl iron complexes†

Randara Pulukkody, Samuel J. Kyran, Michael J. Drummond, Chung-Hung Hsieh, Donald J. Darensbourg and Marcetta Y. Darensbourg*

Received 23rd May 2014
Accepted 16th June 2014

DOI: 10.1039/c4sc01523a

www.rsc.org/chemicalscience

The displacement of RS$^{\bullet}$ from [(NHC)(SPh)Fe(NO)$_2$] (NHC = N-heterocyclic carbene) by carbon monoxide follows associative kinetics, rate = k [CO]^1 [(NHC)(SPh)Fe(NO)$_2$]^1, resulting in reduction of the oxidized form of the dinitrosyliron unit, {Fe(NO)$_2$}^{9} (Enemark–Feltham notation) to {Fe(NO)$_2$}^{10}. Thermodynamically driven by the release of PhS–SPh concomitant with formation of [(NHC)(CO)Fe(NO)$_2$], computational studies suggested the reactant dinitrosyliron unit serves as a nucleophile in the initial slanted interaction of the π^* orbital of CO, shifting into normal linear Fe–CO with weakening of the Fe–SPh bond. The current study seeks to experimentally test this proposal. A series of analogous {Fe(NO)$_2$}^{9} [(NHC)(p-S–C$_6$H$_4$X)Fe(NO)$_2$] complexes, with systematic variation of the *para*-substituents X from electron donor to electron withdrawing groups was used to monitor variation in electron density at the Fe(NO)$_2$ unit *via* Hammett analyses. Despite the presence of non-innocent NO ligands, data from ν(NO) IR spectroscopy and cyclic voltammetry showed consistent tracking of the electron density at the {Fe(NO)$_2$} unit in response to the aryl substituent. The electronic modifications resulted in systematic changes in reaction rates when each derivative was exposed to CO. A plot of the rate constants and the Hammett parameter σ_p is linear with a negative slope and a ρ value of −0.831; such correlation is indicative of rate retardation by electron-withdrawing substituents, and provides experimental support for the unique role of the delocalized frontier molecular orbitals of the Fe(NO)$_2$ unit.

Introduction

That diatomic molecules in combination with metals play vital roles in a variety of physiological functions is well established. While physiologically beneficial carbon monoxide and nitric oxide concentrations are in picomolar to nanomolar range, increasing concentrations result in cytotoxic effects.[1–3] Under physiological control CO and NO function as important regulatory and signaling molecules, and are members of a class of endogenously-produced gaseotransmitters.[4–7] Much current research is directed at the fundamental biochemistry especially significant in the cardiovascular system, as well as development of compounds as pro-drugs, capable of controlled delivery and release of NO and CO to biological targets—the most important in vasodilation activity being iron in porphyrin environments.[8] As an extensive literature exists for transition metal complexes containing CO and NO, much attention has been directed towards appropriate combinations of ligands and metals designed for specific pharmacological properties.[9] Indeed, explorations of one class of complexes, dinitrosyl iron complexes (DNICs), are inspired by their natural occurrence,[10] and by the intriguing proposal that they might be the "most abundant nitric oxide-derived cellular adduct", *i.e.*, superceding the *S*-nitrosothiols (RSNOs).[11] Others have posited that synthetic versions may be developed as NO-release agents.[12]

The chemical properties of CO and NO as ligands to metals are substantially different; the former is viewed as an innocent ligand with weak σ-donor/strong π-acceptor properties in its M–CO bond formation.[13] In contrast, the radical character of NO imparts reactivity that surpasses that of CO, in that its ability to readily switch between the NO$^+$, $^{\bullet}$NO, and NO$^-$ forms depends on the redox levels accessible by the metal to which it binds, thereby defining non-innocent ligand binding.[14]

The lifetime of free NO in the aerobic cellular milieu is reported to be too short to account for its observed physiological functions.[15] Therefore, it is expected that transitory derivatives of NO serve for storage, transport and delivery of NO to required sites. Both organic (RSNOs) and inorganic dinitrosyl iron complexes have been proposed for such NO storage/transport functions *in vivo*.[16,17] The biological DNICs are derived *in vivo*

Department of Chemistry, Texas A & M University, College Station, TX 77843, USA. E-mail: marcetta@chem.tamu.edu

† Electronic supplementary information (ESI) available: Experimental methods, additional spectroscopic, cyclic voltammetric and kinetic details, X-ray crystallographic data (CIF) from the structure determination and full list of metric parameters for complexes **1a–1e**. CCDC 1004078–1004081. For crystallographic data in CIF or other electronic format see DOI: 10.1039/c4sc01523a

Published on 16 June 2014. Downloaded by Tamkang University Libraries on 14/04/2015 07:55:44.

from the labile or cellular chelatable iron pool, or by degradation of iron sulfur clusters; the latter generates protein-bound (cysteinyl-*S*)$_2$Fe(NO)$_2$, as high molecular weight, HMW, moieties.[11,18–22] Characterized by a prominent EPR signal at 2.03,[10,12] the HMW form may be rendered mobile in low molecular weight, LMW, forms on exchange with free cysteine or other thiolate-rich biomolecules such as glutathione.[23] That glutathione-*S* transferase may serve as a Fe(NO)$_2$ transport vehicle has been supported by the isolation and structural characterization of the protein with glutathione–Fe(NO)$_2$ imbedded within its glutathione-binding site.[24]

Numerous small molecule models assumed to be relevant to biological DNICs have been synthesized and characterized.[16,25] Synthetic DNIC complexes exist in two redox levels: oxidized, EPR active {Fe(NO)$_2$}^{9} and the reduced, EPR silent {Fe(NO)$_2$}^{10} (Enemark–Feltham notation).[26] The oxidized form can be found in the neutral L(X)Fe(NO)$_2$ (where for example X = halides, pseudo halides, or thiolate S-donors and L = N-donors or the good sigma donor ligands N-heterocyclic carbenes (NHC) that are apt analogues of imidazoles), and the anionic X$_2$Fe(NO)$_2^-$ complexes.[27–31] The reduced form can be found in the L$_2$Fe(NO)$_2$ state, with the paradigm being the 18-electron species, (OC)$_2$Fe(NO)$_2$, a versatile precursor to LFe(CO)(NO)$_2$ derivatives.[27,32–35] The ligand environment is critical in stabilizing the redox state of the DNIC which in turn is expected to govern its endogenous role as NO storage or releasing agent.[31] While there exists a variety of four-coordinate {Fe(NO)$_2$}^{9} synthetic DNIC models in the inorganic chemistry literature, several reports have also presented the rare, five-coordinate counterparts.[36–38] Our work focuses on developing understanding of mixed ligand environments and mechanisms of ligand exchange processes that might regulate switches in redox levels.

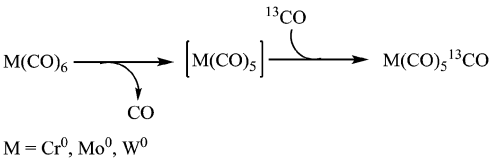

(1)

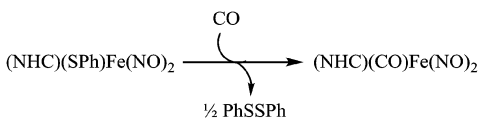

(2)

$$\text{Rate} = k_2\,[\text{CO}]^1\,[(\text{NHC})(\text{SPh})\text{Fe}(\text{NO})_2]^1$$

$$\Delta H^{\ddagger} = 7.80 \pm 0.16 \text{ kcal mol}^{-1} \text{ and } \Delta S^{\ddagger} = -45.0 \pm 0.5 \text{ e.u.}$$

As a poor nucleophile, CO exchange reactions with a metal-bound CO or L typically take place by dissociative mechanisms allowing external CO to be trapped by an open site as in eqn (1).[39] Recently we reported an example of CO displacement of RS$^{\bullet}$ in a dinitrosyliron complex, the kinetics of which followed a second-order rate expression with activation parameters

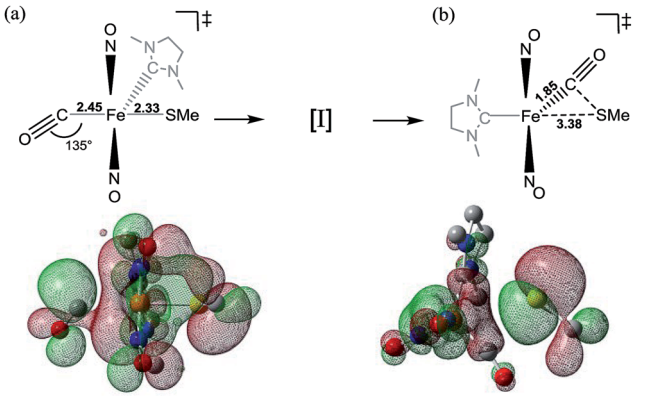

Fig. 1 (Top) (a) A sketch of the calculated collision complex,[40] involved in the rate determining step for CO and (NHC)(RS)Fe(NO)$_2$, proceeding through a 5-coordinate intermediate I.[40] Theory finds that as the Fe–CO bond becomes linear as in (b), the Fe–SR bond lengthens, and releases a thiyl radical, either by direct homolytic Fe–S bond cleavage or *via* homolytic C–S cleavage from a transient metallothioester group.[40] (Bottom) Corresponding plots of the transition state SOMOs: (a) the unpaired electron on the {Fe(NO)$_2$} donates into the π* orbital of the side-on entering CO; and (b) the shift of the unpaired electron releases thiyl radical.[40]

consistent with an associative mechanism, eqn (2).[40] This process entailed a change in the redox state of the reactant DNIC as the oxidized state, {Fe(NO)$_2$}^{9}, converted into the reduced analogue, {Fe(NO)$_2$}^{10}. Proceeding under mild conditions, the thermodynamics of the reaction is driven by the formation of RSSR as a result of the release of RS$^{\bullet}$. Computational studies were carried out in pursuit of a reasonable mechanistic proposal for the observed reactivity, resulting in the suggestion that the π-density of the {Fe(NO)$_2$} unit was involved in nucleophilic attack on CO, the latter acting as an electrophile, Fig. 1.[40] Theory suggested a side-on approach of CO leading to a 5-coordinate intermediate, species I of Fig. 1, with the NO ligands accommodating the excess charge. Such nucleophilicity of the iron in {Fe(NO)$_2$}, especially in the oxidized {Fe(NO)$_2$}^{9}, was unexpected.[40]

Herein we report experiments designed to test the mechanistic proposal that had suggested such a unique role of the {Fe(NO)$_2$} unit in the CO – induced disulfide elimination. We have prepared a series of analogous {Fe(NO)$_2$}^{9} [(NHC)(*p*-*S*C$_6$H$_4$X)Fe(NO)$_2$] complexes, where the *para*-substituents X were systematically varied from electron donor to electron withdrawing groups that might be used in a Hammett analysis of their effects on electron density at the Fe(NO)$_2$ unit. Data from ν(NO) IR spectroscopy and cyclic voltammetry was used to track the differences of the electron density at the {Fe(NO)$_2$} unit in response to the aryl substituent. Systematic changes were observed in the rates of reaction when each derivative was exposed to CO, consistent with the electronic changes at the Fe(NO)$_2$ unit.

Results and discussion

Synthesis and isolation

A series of dinitrosyliron complexes containing *para*-substituted aryl thiolates, (sIMes)(S–C$_6$H$_4$X)Fe(NO)$_2$ (compounds **1a–1e**)

 This journal is © The Royal Society of Chemistry 2014

Published on 16 June 2014. Downloaded by Tamkang University Libraries on 14/04/2015 07:55:44.

was synthesized by homolytic cleavage of the corresponding Roussin's Red Ester (**RRE**), $(\mu\text{-}(S\text{–}C_6H_4X))_2[Fe(NO)_2]_2$ (ref. 42) by two equivalents of the sIMes ligand (freshly prepared by combining 1,3-bis(2,4,6-trimethylphenyl)imidazolinium chloride and NaO^{t}Bu in a 1 : 1 stoichiometric ratio). Scheme 1 shows the synthetic protocol along with Hammett parameters for the substituents of the *p*-SC_6H_4X series. The brown **RRE** solution changed to blue/purple, from which purple solids were isolated upon recrystallization with cold hexane.

The DNICs **1a–1e** were stable under inert atmosphere for several months in the solid state. In solution, under inert atmosphere, stability was diminished to 2–3 weeks. Four members of the series (**1a**, **1b**, **1c** and **1e**) were characterized by X-ray crystallography and their molecular structures are compared in Fig. 2. X-ray quality crystals of **1b** and **1c** were obtained by slow evaporation of concentrated ether solutions, while those of **1a** and **1e** were obtained from solutions of THF–hexane. Table 1 lists selected bond distances and angles for **1a**, **1b**, **1c** and **1e**. Crystals of the complex **1d** have thus far eluded crystallization.

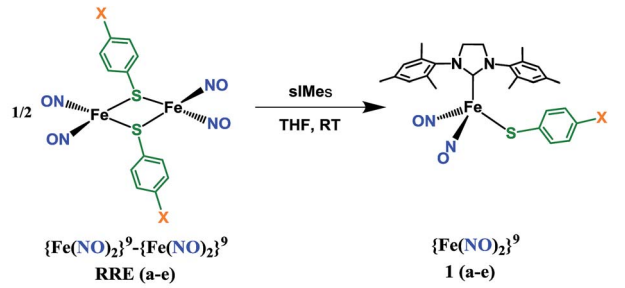

$\{Fe(NO)_2\}^9$-$\{Fe(NO)_2\}^9$ RRE (a-e) $\{Fe(NO)_2\}^9$ 1 (a-e)

	a	b	RRE/1	c	d	e
X	OCH_3	CH_3	H	Cl	CF_3	NO_2
σ_p[41]	-0.268	-0.170	0.000	0.230	0.540	0.778

Scheme 1

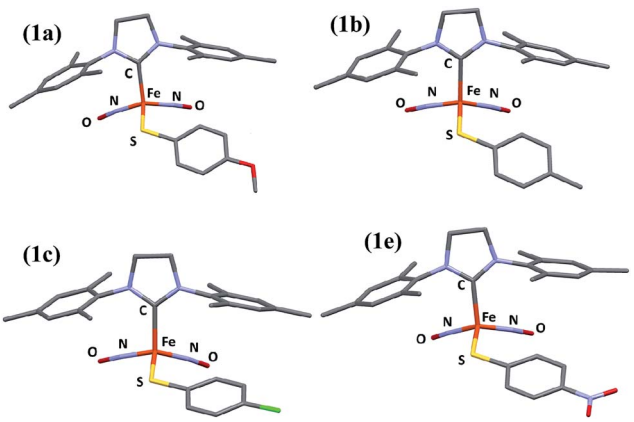

Fig. 2 Molecular structures of **1a**, **1b** (cyclohexane packing solvent omitted for clarity), **1c** and **1e**, from X-ray diffraction analysis. Thermal ellipsoid plots and full lists of metric parameters are provided in the ESI.†

Table 1 Selected bond distances and angles in $[(sIMes)(S\text{–}C_6H_4X)Fe(NO)_2]$ complexes **1a**, **1b**, **1c** and **1e**[a]

	1a X = OCH_3	**1b** X = CH_3	**1c** X = Cl	**1e** X = NO_2
Bond distances (Å)				
Fe–C	2.052(2)	2.049(2)	2.048(2)	2.044(2)
Fe–NO[a]	1.672(2)	1.674(1)	1.675(2)	1.673(2)
Fe–S	2.243(1)	2.239(1)	2.248(1)	2.259(1)
N–O	1.177(2)	1.172(2)	1.176(2)	1.172(2)
	1.178(2)	1.175(2)	1.168(2)	1.172(3)
Bond angles (deg.)				
N–Fe–N	115.5(1)	115.4(1)	116.8(1)	110.9(1)
Fe–N–O	167.4(1)	168.6(1)	169.5(1)	165.7(1)
	169.0(1)	167.8(1)	169.7(2)	163.7(2)
C–Fe–NO[a]	106.0(1)	106.3(1)	106.0(1)	106.0(1)
C–Fe–S	112.0(1)	109.5(1)	109.1(1)	107.5(1)

[a] Average distance or angles. The maximum deviations from the average distances and angles are shown in the table. Full lists of metric parameters are available in the ESI.

The complexes in Fig. 1 are tetrahedral wherein the CN_2C_2 plane of the sIMes bisects the S–Fe–N angles of the trigonal base; that is, the NHC plane does not eclipse the Fe–N or Fe–S bond vectors. The planes of the mesitylenes are roughly perpendicular to the CN_2C_2 plane and appear to umbrella the $Fe(NO)_2SR$ motif. All structures maintain the previously described "attracto" conformation[35] where the two Fe–N–O with slight deviations from linearity, are oriented towards each other. The Fe–N–O angles and all other metric parameters of structures **1a**, **1b**, **1c** and **1e** are comparable to each other and to those of the $[(sIMes)(SPh)Fe(NO)_2]$ analogue.[40] Although barely within significant limits, there appears to be a gradual decrease of Fe–C_{NHC} bond lengths with the electron withdrawing ability of the *para* substituent on the S–C_6H_4, concomitant with an increase in the Fe–S bond distance. This correlation is further reflected in the ν(NO) vibrational spectra.

Infrared spectroscopy

Noticeable shifts in the positions of the ν(NO) bands in the solution IR spectra allowed monitoring of the complete conversion of the **RRE** precursor to the corresponding dinitrosyl iron monomers. The ν(NO) positions of both the **RRE(a–e)** series and the DNIC series (**1a–1e**), showed small but systematic shifts to lower wavenumbers over an overall range of *ca.* 12 cm^{-1} when the *para* substituent was varied from electron-withdrawing groups (EWGs) to electron-donating groups (EDGs), in agreement with arguments of π-back bonding (Fig. 3). Analysis of the ν(NO) positions and their correspondence to the *para* substituent on the –SC_6H_4X using the Hammett parameter[41] σ_p is given in Fig. 3. The unsubstituted analogues (where X = H), the **RRE** $[(\mu\text{-}(S\text{–}C_6H_5))_2[Fe(NO)_2]_2]$, and complex **1** $[(sIMes)(SPh)Fe(NO)_2]$, are also included in the above analysis.[40]

Assuming idealized C_{2v} symmetry, the ν(NO) values were used to calculate the relevant NO force constants using an analogous process to that developed by Cotton–Kraihanzel for CO stretching force constants (eqn (3) and (4)),[43,44] where k_1 is the NO stretching force constant and k_c is the interaction

Published on 16 June 2014. Downloaded by Tamkang University Libraries on 14/04/2015 07:55:44.

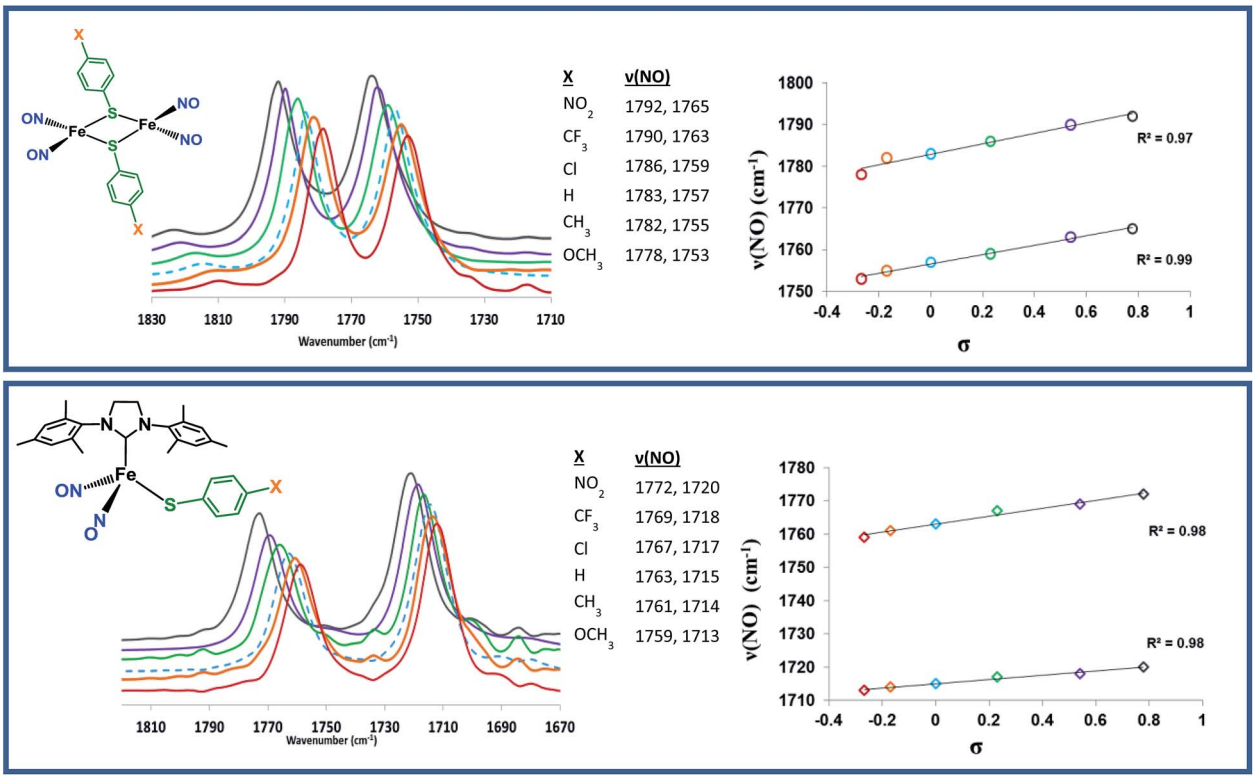

Fig. 3 Top panel (left) overlaid IR spectra for **RRE**, **RRE(a–e)**; (right) plots of the two ν(NO) bands for **RRE**, **RRE(a–e)** *vs.* the Hammett substituent parameter σ_p. Bottom panel (left) overlaid IR spectra for **1**, **1a–1e**; (right) plots of the two ν(NO) bands for **1**, **1a–1e** *vs.* the Hammett substituent parameter σ_p. **a** (red), **b** (brown), **1**/**RRE** (blue; dashed line), **c** (green), **d** (purple), **e** (grey).

constant, Table 2. Fig. 4 shows a plot of the calculated force constants (k_1) and the Hammett parameter σ_p. Thus, although remote from the metal, the X substituent on the aryl group has a subtle but systematic effect on the electron density at the metal center, as reported by the ν(NO) values.

$$\lambda_1 = \mu\,(k_1 + k_c) \quad (3)$$

$$\lambda_2 = \mu\,(k_1 - k_c) \quad (4)$$

where

$$\lambda = (5.8890 \times 10^{-2})\nu^2$$

Table 2 Summary of characterization data used to obtain Hammett correlations of complexes **1a–1e**

Complex	*p*-X substituent	ν(NO) cm^{-1} (THF) Sym	Asym	Force constant (k_1) (mdyne Å^{-1})	$E_{1/2}$[a] (mV)
1a	OCH_3	1759	1713	13.26	−1.44
1b	CH_3	1761	1714	13.28	−1.41
1	H	1763[b]	1715[b]	13.30	−1.40
1c	Cl	1767	1717	13.35	−1.33
1d	CF_3	1769	1718	13.37	−1.30
1e	NO_2	1772	1720	13.41	−1.19

[a] $E_{1/2}$ values are referenced to Cp_2Fe/Cp_2Fe^+. [b] Previous work.[40]

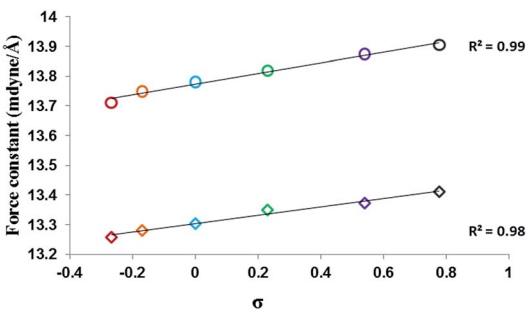

Fig. 4 Plots of force constant (k_1) for (top, circles) **RRE**, **RRE(a–e)** and (bottom, diamonds) **1**, **1a–1e** *vs.* the Hammett substituent parameter σ_p.

EPR spectroscopy

The EPR spectra of complexes **1a–1e** were recorded in THF solution at 295 K. All complexes display broad rhombicity in the EPR signal, with observed *g* values: $g_1 = 2.027$, $g_2 = 2.024$, $g_3 = 2.020$ (see ESI† for a representative EPR spectrum). Varying the substituent at the *para* position does not appear to affect the EPR derived *g* value of these complexes.

Electrochemistry

The electronic effect of the X-substituent of the $-SC_6H_4X$ series as interpreted from the ν(NO) IR values is also reflected

 This journal is © The Royal Society of Chemistry 2014

Published on 16 June 2014. Downloaded by Tamkang University Libraries on 14/04/2015 07:55:44.

in the electrochemistry. The unsubstituted analogue, complex **1** [(sIMes)(SPh)Fe(NO)$_2$], shows a reversible redox event at −1.39 V (in THF solution), which is assigned to the {Fe(NO)$_2$}$^{9/10}$ couple, similar to the previously reported IMes analogue.[27] Reversibility is indicated by an i_{pa}/i_{pc} ratio of 0.997 (at a scan rate of 100 mV s^{-1}), and is scan-rate-independent in the range 75 to 250 mV s^{-1}, see ESI.† For **1**, the ΔE_p value is ∼226 mV. However, under these conditions, the Fc/Fc$^+$ standard also shows similar separation (see ESI†), again indicating good reversibility.

All other derivatives in the series show similar reversible redox events (scan-rate-independent; see ESI†), also assigned to the {Fe(NO)$_2$}$^{9/10}$ redox couple. These events range from −1.19 V to −1.44 V for the –NO$_2$, –CF$_3$, –Cl, –CH$_3$ and –OCH$_3$ derivatives respectively. The trend in the $E_{1/2}$ is as expected, shifting to higher negative potentials when moving from electron withdrawing groups to electron donating groups (Fig. 5). There is good correlation between $E_{1/2}$ and the Hammett parameter σ_p as shown in Fig. 6. Also correlating with the ν(NO) values and force constants, these $E_{1/2}$ values are therefore indicative of the changes in electron density occurring at the Fe(NO)$_2$ unit upon changes in the substituent at a remote position. Table 2 summarizes the characterization data used to obtain Hammett correlations of complexes **1a–1e**.

Fig. 7 compares the single reversible redox event for **1c** (Fig. 7(i)) as representative of all members of the series as opposed to the *p*-NO$_2$ derivative, **1e** (Fig. 7(ii)). For the latter, the reversible redox event centered at −1.19 V is assigned to the {Fe(NO)$_2$}$^{9/10}$ redox couple in accordance with the occurrence of the same redox event for other derivatives in this range of potentials (Fig. 7(i), **1c**). A second reversible event appears at −2.10 V. The latter is assigned to a redox event involving the nitro group of the S(C$_6$H$_4$–NO$_2$) ligand. Support for this assignment is as follows: Fig. 7(iii) displays the cyclic voltammogram of an authentic sample of bis(4-nitrophenyl) disulfide. The unusual shape is typical of aromatic disulfides in the −500 to −1500 mV range and it is fully reproducible.[45–48] Considering the above, the nearly reversible feature centered around −2.10 V for both bis(4-nitrophenyl) disulfide and **1e** is assigned to a reduction involving the –NO$_2$ group. The small features between the two major redox events in the voltammogram of **1e** are present regardless of the scan direction and still appear when reverse scans are initiated. We have thus far been unable to assign these features to specific redox events.

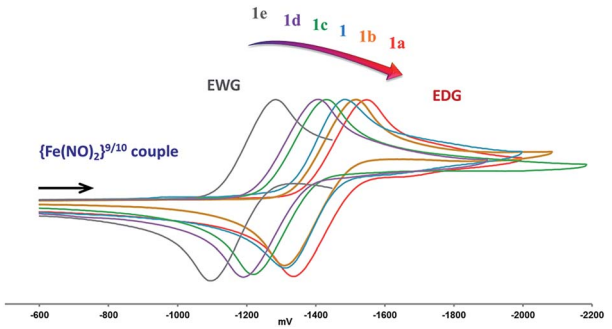

Fig. 5 Overlaid cyclic voltammograms (THF solution, scan rate 100 mV s^{-1}, 100 mM [*n*-Bu$_4$N][PF$_6$] as supporting electrolyte) of **1a** (red), **1b** (brown), **1** (blue), **1c** (green), **1d** (purple), **1e** (grey; full voltammogram shown in Fig. 7(ii)). All are referenced to Cp$_2$Fe/Cp$_2$Fe$^+$.

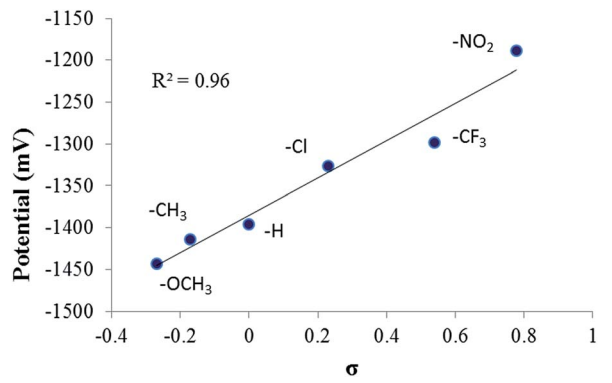

Fig. 6 Plot of $E_{1/2}$ for **1a–1e** *vs.* the Hammett substituent parameter σ_p. All are referenced to Cp$_2$Fe/Cp$_2$Fe$^+$.

Kinetic measurements

The rates of conversion of complexes **1a–1e** to **2**, were examined using *in situ* IR spectroscopy (Scheme 2). All iron complexes

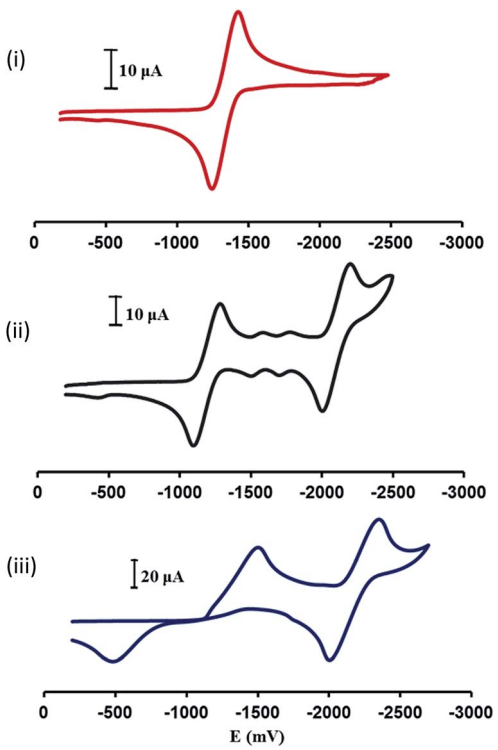

Fig. 7 Cyclic voltammograms of (i) **1c** (ii) **1e** and (iii) bis(4-nitrophenyl) disulfide at scan rates of 100 mV s^{-1} in THF (100 mM [*n*-Bu$_4$N][PF$_6$] as supporting electrolyte). All are referenced to Cp$_2$Fe/Cp$_2$Fe$^+$.

Published on 16 June 2014. Downloaded by Tamkang University Libraries on 14/04/2015 07:55:44.

were subject to pseudo-first-order reaction conditions under an excess of CO and the rate constants, k, of each reaction were derived from the respective linear natural log plots (eqn (5)). A reaction monitor and its respective natural log plot for the reaction between **1b** and CO are shown in Fig. 8. The kinetic profiles of **1a–1e** are similar to that of the closely related unsubstituted analogue, complex **1**, reported earlier.[40] Therefore it is reasonable to assume that the reaction follows a similar second order rate expression, first order in each reagent, eqn (5).

$$\text{Rate} = k_{obs}\,[\text{Fe}], \text{ where } k_{obs} = k\,[\text{CO}] \quad (5)$$

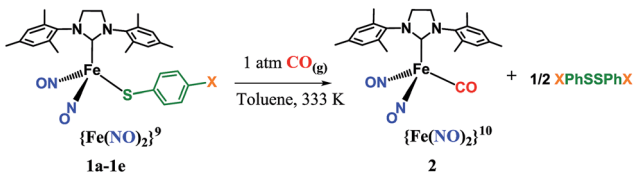

Scheme 2

Rate constants (k) and $t_{1/2}$ values are listed in Table 3, and indicate that the stronger the electron-withdrawing group on the phenyl thiolate, the slower the formation of the product carbonyl complex, **2**. In the case of the nitro species, **1e** the reaction time is longer than the solution life-time of the reagent, as such, significant decomposition is observed with the progress of the reaction. It is likely that the decomposed species may induce further decomposition in the product, and in fact this is observed by the decrease in product intensity over time. Thus, only the first 10% of the reaction data, which is linear upon logarithmic treatment, was used to calculate the rate constant for **1e**. Though the error in rate measurement could be higher, it can be concluded to have a slower rate than seen for the other complexes. Decomposition was also observed with the trifluoromethane species, **1d** the next strongest electron-withdrawing group in the series, but to a smaller extent. A slight deviation in the trend is seen with the methyl derivative, **1b** where its rate is comparable with the unsubstituted species in this series, **1** or (sIMes)(SPh)$Fe(NO)_2$.

A plot of the rate constants and the Hammett parameter σ_p is linear with a negative slope and a ρ value of −0.831 with an R^2 of 0.901; such correlation is indicative of rate retardation by electron-withdrawing substituents (Fig. 9). The nitro species has been omitted for reasons mentioned above, but its inclusion gives a ρ value of −1.293 and an R^2 of 0.869 (see ESI†). The ρ value is an indicator of change in charge during the rate-determining step, and its negative value implies a diminution of negative charge at the reaction center. This agrees with our prior computational work,[40] where there is loss of negative charge at the $Fe(NO)_2$ unit as a result of its initial nucleophilic attack on an incoming CO molecule. *Thus, the facilitation of this reaction by electron-releasing substituents is supportive of the proposed mechanism.*

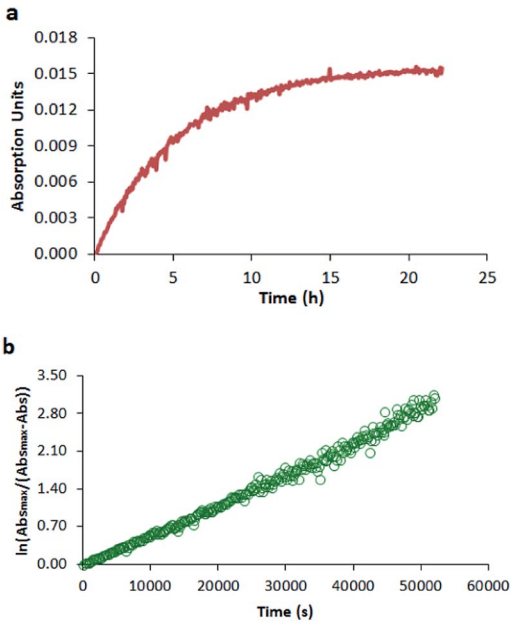

Fig. 8 (a) Infrared reaction profile of **2**, monitored at ν(CO) = 1992 cm^{-1}, upon formation in a toluene solution of [(sIMes)(S–C_6H_4–CH_3)$Fe(NO)_2$], **1b**, and CO at 333 K. (b) Natural log plot of absorption data *versus* time showing linear trend over three half-lives. The R^2 value is 0.991.

Table 3 Kinetic parameters for reactions of **1a–1e** with CO obtained from linear fits of natural log plots

Complex	Substituent	$k_{obs} \times 10^3$ (s^{-1})	$k \times 10^3$ (M^{-1} s^{-1})	$t_{1/2}$ (h)
1a[a]	OCH_3	0.103 ± 0.012	12.9 ± 1.5	1.9
1b[a]	CH_3	0.0555 ± 0.0030	6.95 ± 0.38	3.5
1 (ref. 40)	H	0.0603	7.56	3.2
1c	Cl	0.0424	5.31	4.5
1d[b]	CF_3	0.0172	2.16	11.2
1e[b]	NO_2	0.00270	0.338	71.4

[a] Average of 3 trials. [b] Rates based on first 10% of data due to decomposition of reaction mixture over time.

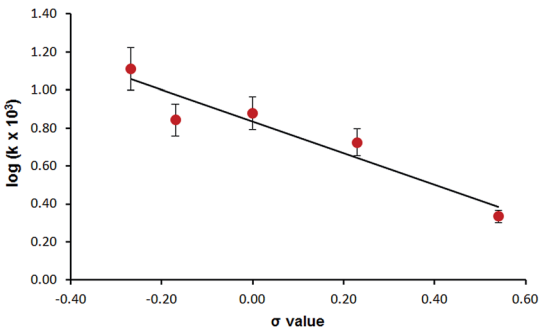

Fig. 9 Hammett plot of rate constants from reactions of DNICs (**1a–1d**, **1**) with CO. Error bars are 10% of original value. Slope of trend line is −0.831 with an R^2 of 0.901.

This journal is © The Royal Society of Chemistry 2014

Published on 16 June 2014. Downloaded by Tamkang University Libraries on 14/04/2015 07:55:44.

Conclusions

For visualizing relationships between structure and reactivity, Hammett correlations are a hallmark of physical organic and physical organometallic chemistry. Such correlations in a series of *para* substituted [(sIMes)(S–C_6H_4X)Fe$(NO)_2$] DNICs (compounds **1a–1e**) with variations in the donor characteristics of the aryl thiolate were used to provide a firmer experimental foundation for the unusual theoretical proposal that an oxidized {Fe$(NO)_2$} moiety, *i.e.* {Fe$(NO)_2$}^{9}, served as a nucleophile towards CO in a process that releases RSSR.[40] Significant electronic rearrangement leads to a reduced {Fe$(NO)_2$} product in the form of [Fe(CO)$(NO)_2$(NHC)].

Although variation of the substituent at the *para* position of the phenyl thiolate takes place remote from the metal center of the {Fe$(NO)_2$}^{9} core, plots of infrared ν(NO) values, calculated NO force constants and voltammetric $E_{1/2}$ values with the Hammett parameter σ_p show good correlations, verifying the presence of systematic changes in electron density as experienced by the {Fe$(NO)_2$}^{9} core through changes in the S-donor. Having thus established the presence of electronic changes at the metal center between the members of the series of DNICs **1a–1e**, rates of their reaction with CO, resulting in the formation of the reduced {Fe$(NO)_2$}^{10} DNIC, [(sIMes)(CO)Fe$(NO)_2$] were examined as monitored by *in situ* IR spectroscopy. A plot of the second-order rate constants and the Hammett parameter σ_p is linear and has a negative slope, indicative of rate retardation with increasing electron-withdrawing nature of the substituents. Together, these results find that subtle, systematic alterations of the electronic character of the {Fe$(NO)_2$} unit moderate the conversion of the {Fe$(NO)_2$}^{9} into the reduced analogue {Fe$(NO)_2$}^{10} under mild conditions.

As reported in the earlier, prototypical study, the calculated free energy of the transition state is close to that of the intermediate,[40] suggesting a late transition state.[49] Experimental results obtained in our current study show that this reaction is sensitive to the nucleophilicity at the metal center, thereby indicating the importance of the CO interaction in the transition state. This study therefore supports the previous computationally derived mechanistic hypothesis of the unique role of the delocalized frontier molecular orbitals of the Fe$(NO)_2$ unit, whereby the reaction is initiated by the overlap of such filled orbitals with the vacant π^* orbitals of the entering CO ligand.[40]

As "cross-talk" between small endogenous gaseotransmitters: CO, NO and H_2S gains rapid interest in the scientific community,[8] the interplay between these molecules and bio-organometallic entities such as DNICs is intriguing. Efforts to understand these processes in the complex biological environment continues to be a challenge, highlighting the importance of the mechanistic understanding obtained in biomimetic studies.

Acknowledgements

We are thankful for financial support from the National Science Foundation (CHE-1266097 to M.Y.D., CHE-1057743 to D.J.D.), and the Robert A. Welch Foundation (A-0924 to M.Y.D., A-0923 to D.J.D.). Michael J. Drummond was supported in the summer 2013 REU program at TAMU (CHE-1062840). The authors acknowledge Dr Nattamai Bhuvanesh of the X-ray Diffraction laboratory and Ryan D. Bethel at Texas A&M University for helpful discussions.

Notes and references

1 M. R. Miller and I. L. Megson, *Br. J. Pharmacol.*, 2007, **151**, 305–321.
2 J. C. Toledo and O. Augusto, *Chem. Res. Toxicol.*, 2012, **25**, 975–989.
3 L. Wu and R. Wang, *Pharmacol. Rev.*, 2005, **57**, 585–630.
4 R. F. Furchgott, *Biosci. Rep.*, 1999, **19**, 235–251.
5 L. J. Ignarro, *Biosci. Rep.*, 1999, **19**, 51–71.
6 F. Murad, *Biosci. Rep.*, 1999, **19**, 133–154.
7 C. Szabo, *Sci. Transl. Med.*, 2010, **2**, 54.
8 M. Kajimura, R. Fukuda, R. M. Bateman, T. Yamamoto and M. Suematsu, *Antioxid. Redox Signaling*, 2010, **13**, 157–192.
9 B. E. Mann and R. Motterlini, *Chem. Commun.*, 2007, 4197–4208.
10 A. F. Vanin, *Nitric Oxide: Biology and Chemistry*, 2009, **21**, 1–13.
11 J. R. Hickok, S. Sahni, H. Shen, A. Arvind, C. Antoniou, L. W. M. Fung and D. D. Thomas, *Free Radical Biol. Med.*, 2011, **51**, 1558–1566.
12 A. F. Vanin and E. I. Chazov, *Biofizika*, 2011, **56**, 304–315.
13 R. H. Crabtree, *The organometallic chemistry of the transition metals*, Wiley, New York, 5th edn., 2009, ch. 4, p. 88.
14 J. S. Stamler, D. J. Singel and J. Loscalzo, *Science*, 1992, **258**, 1898–1902.
15 D. D. Thomas, X. Liu, S. P. Kantrow and J. R. Lancaster, Jr, *Proc. Natl. Acad. Sci. U. S. A.*, 2001, **98**, 355–360.
16 H. Lewandowska, M. Kalinowska, K. Brzoska, K. Wojciuk, G. Wojciuk and M. Kruszewski, *Dalton Trans.*, 2011, **40**, 8273–8289.
17 A. R. Butler and I. L. Megson, *Chem. Rev.*, 2002, **102**, 1155–1166.
18 J. C. Toledo, C. A. Bosworth, S. W. Hennon, H. A. Mahtani, H. A. Bergonia and J. R. Lancaster, *J. Biol. Chem.*, 2008, **283**, 28926–28933.
19 B. D'Autreaux, O. Horner, J. L. Oddou, C. Jeandey, S. Gambarelli, C. Berthomieu, J. M. Latour and I. Michaud-Soret, *J. Am. Chem. Soc.*, 2004, **126**, 6005–6016.
20 H. W. Foster and J. A. Cowan, *J. Am. Chem. Soc.*, 1999, **121**, 4093–4100.
21 M. C. Kennedy, W. E. Antholine and H. Beinert, *J. Biol. Chem.*, 1997, **272**, 20340–20347.
22 M. H. Lee, P. Arosio, A. Cozzi and N. D. Chasteen, *Biochemistry*, 1994, **33**, 3679–3687.
23 A. Mulsch, P. Mordvintcev, A. F. Vanin and R. Busse, *FEBS Lett.*, 1991, **294**, 252–256.
24 E. Cesareo, L. J. Parker, J. Z. Pedersen, M. Nuccetelli, A. P. Mazzetti, A. Pastore, G. Federici, A. M. Caccuri, G. Ricci, J. J. Adams, M. W. Parker and M. Lo Bello, *J. Biol. Chem.*, 2005, **280**, 42172–42180.

Published on 16 June 2014. Downloaded by Tamkang University Libraries on 14/04/2015 07:55:44.

25 C. T. Tran, K. M. Skodje and E. Kim, *Prog. Inorg. Chem.*, 2014, **59**, 339–380.
26 J. H. Enemark and R. D. Feltham, *Coord. Chem. Rev.*, 1974, **13**, 339–406.
27 J. L. Hess, C. H. Hsieh, J. H. Reibenspies and M. Y. Darensbourg, *Inorg. Chem.*, 2011, **50**, 8541–8552.
28 H. W. Huang, C. C. Tsou, T. S. Kuo and W. F. Liaw, *Inorg. Chem.*, 2008, **47**, 2196–2204.
29 T. T. Lu, C. C. Tsou, H. W. Huang, I. J. Hsu, J. M. Chen, T. S. Kuo, Y. Wang and W. F. Liaw, *Inorg. Chem.*, 2008, **47**, 6040–6050.
30 Z. J. Tonzetich, L. H. Do and S. J. Lippard, *J. Am. Chem. Soc.*, 2009, **131**, 7964–7965.
31 F. T. Tsai, S. J. Chiou, M. C. Tsai, H. W. Huang, M. H. Chiang and W. F. Liaw, *Inorg. Chem.*, 2005, **44**, 5872–5881.
32 M. L. Tsai, C. H. Hsieh and W. F. Liaw, *Inorg. Chem.*, 2007, **46**, 5110–5117.
33 F. L. Atkinson, H. E. Blackwell, N. C. Brown, N. G. Connelly, J. G. Crossley, A. G. Orpen, A. L. Rieger and P. H. Rieger, *J. Chem. Soc., Dalton Trans.*, 1996, 3491–3502.
34 D. W. Mcbride, S. L. Stafford and F. G. A. Stone, *Inorg. Chem.*, 1962, **1**, 386–388.
35 N. Reginato, C. T. C. McCrory, D. Pervitsky and L. J. Li, *J. Am. Chem. Soc.*, 1999, **121**, 10217–10218.
36 C. H. Chen, Y. C. Ho and G. H. Lee, *J. Organomet. Chem.*, 2009, **694**, 3395–3400.
37 W. C. Shih, T. T. Lu, L. B. Yang, F. T. Tsai, M. H. Chiang, J. F. Lee, Y. W. Chiang and W. F. Liaw, *J. Inorg. Biochem.*, 2012, **113**, 83–93.
38 D. H. Jo, Y. M. Chiou and L. Que, *Inorg. Chem.*, 2001, **40**, 3181–3190.
39 R. B. Jordan, *Reaction mechanisms of inorganic and organometallic systems*, Oxford university press, Oxford, 3rd edn, 2007, ch. 5, p. 150.
40 R. Pulukkody, S. J. Kyran, R. D. Bethel, C. H. Hsieh, M. B. Hall, D. J. Darensbourg and M. Y. Darensbourg, *J. Am. Chem. Soc.*, 2013, **135**, 8423–8430.
41 J. E. Leffler and E. Grunwald, *Rates and equilibria of organic reactions*, Dover Publications, 1963.
42 T. B. Rauchfuss and T. D. Weatherill, *Inorg. Chem.*, 1982, **21**, 827–830.
43 F. A. Cotton, *Inorg. Chem.*, 1964, **3**, 702–711.
44 C. S. Kraihanzel and F. A. Cotton, *Inorg. Chem.*, 1963, **2**, 533–540.
45 S. Antonello, R. Benassi, G. Gavioli, F. Taddei and F. Maran, *J. Am. Chem. Soc.*, 2002, **124**, 7529–7538.
46 S. Antonello, K. Daasbjerg, H. Jensen, F. Taddei and F. Maran, *J. Am. Chem. Soc.*, 2003, **125**, 14905–14916.
47 K. Daasbjerg, H. Jensen, R. Benassi, F. Taddei, S. Antonello, A. Gennaro and F. Maran, *J. Am. Chem. Soc.*, 1999, **121**, 1750–1751.
48 C. Ji, J. D. Goddard and A. Houmam, *J. Am. Chem. Soc.*, 2004, **126**, 8076–8077.
49 G. S. Hammond, *J. Am. Chem. Soc.*, 1955, **77**, 334–338.

 This journal is © The Royal Society of Chemistry 2014